analytical chemistry

pubs.acs.org/ac Article

Flexible Point-of-Care Electrodes for Ultrasensitive Detection of Bladder Tumor-Relevant miRNA in Urine

Duo Chen,‖ Na Chen,‖ Fangning Liu,‖ Yiming Wang, Huageng Liang, Yanbing Yang,* and Quan Yuan

Cite This: *Anal. Chem.* 2023, 95, 1847−1855 Read Online

ACCESS | Metrics & More | Article Recommendations | Supporting Information

ABSTRACT: Portable point-of-care testing (POCT) is currently drawing enormous attention owing to its great potential for disease diagnosis and personal health management. Electrochemical biosensors, with the intrinsic advantages of cost-effectiveness, fast response, ease of miniaturization, and integration, are considered as one of the most promising candidates for POCT application. However, the clinical application of electrochemical biosensors-based POCT is hindered by the decreased detection sensitivity due to the low abundance of disease-relevant biomolecules in extremely complex biological samples. Herein, we construct a flexible electrochemical biosensor based on single-stranded DNA functionalized single-walled carbon nanotubes (ssDNA-SWNTs) for high sensitivity and stability detection of miRNA-21 in human urine to achieve bladder cancer (BCa) diagnosis and classification. The ssDNA-SWNT electrodes with a 2D interconnected network structure exhibit a high electrical conductivity, thus enabling the ultrasensitive detection of miRNA-21 with a detection limit of 3.0 fM. Additionally, the intrinsic flexibility of ssDNA-SWNT electrodes endows the biosensors with the capability to achieve high stability detection of miRNA-21 even under large bending deformations. In a cohort of 40 BCa patients at stages I−III and 44 negative control samples, the constructed ssDNA-SWNT biosensors could detect BCa with a 92.5% sensitivity, an 88.6% specificity, and classify the cancer stages with an overall accuracy of 81.0%. Additionally, the flexible ssDNA-SWNT biosensors could also be utilized for treatment efficiency assessment and cancer recurrence monitoring. Owing to their excellent sensitivity and stability, the designed flexible ssDNA-SWNT biosensors in this work propose a strategy to realize point-of-care detection of complex clinical samples to achieve personalized healthcare.

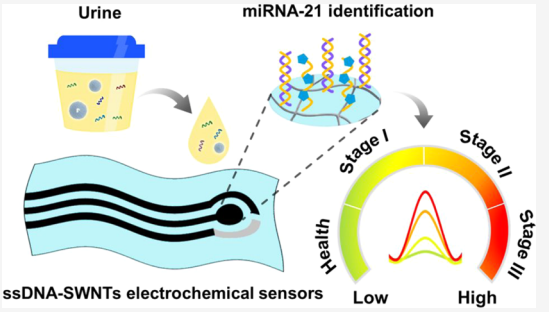

With the ability to realize rapid and low-cost detection of biological samples, portable point-of-care testing (POCT) has attracted enormous interest in the future evolution of personal healthcare and the achievement of health management in resource-limited settings.[1−4] Typically, a POCT device lies on the integration of circuit and microfluidic technologies with a biosensor that could detect target biomolecules and export thermal, optical, or electrical signals.[5−12] Electrochemical biosensors could convert chemical and biological molecules information into readable electrical signals through the interaction between electrodes and analytes. Owing to their intrinsic advantages of cost-effectiveness, fast response, ease of miniaturization, and integration, electrochemical biosensors show great potential in POCT applications.[13−15] However, the clinical POCT applications of electrochemical biosensors are hindered by the decreased detection sensitivity and reliability in extremely complex biological samples with low-abundance target biomolecules.[16,17] Consequently, the development of electrochemical biosensors with high sensitivity and stability is of great significance for clinical POCT applications.[18−20]

As the key element of electrochemical biosensors, the sensing electrode that was directly in contact with target biomolecules plays key roles in determining the detection sensitivity and stability.[21−23] The sensing electrodes with high electrical conductivity and mechanical flexibility could enable efficient and stable electrochemical signal conduction even under mechanical deformations, thus ensuring detection sensitivity and stability.[24−26] One-dimensional (1D) nanostructures, such as nanowires and nanotubes, are supposed to offer straightforward nanochannels for fast electron transport, promising their excellent electrical conductivity.[27,28] Besides, 1D nanostructures could be cross-linked into two-dimensional (2D) network structured electrodes with low contact resistance, thus offering an electrical conduction pathway to achieve high sensitivity in clinical POCT applications.[29,30] More importantly, the interconnected network structure could transfer loading strain effectively under large bending deformation to ensure the mechanical integrity and electrical conductivity of the whole structure.[31,32] In this regard, 2D

Received: July 21, 2022
Accepted: December 30, 2022
Published: January 6, 2023

https://doi.org/10.1021/acs.analchem.2c03156
Anal. Chem. 2023, 95, 1847−1855

flexible network structured electrodes that were cross-linked by conductive 1D nanowires might offer a pathway to achieve high sensitivity and stability point-of-care detection of complex clinical biological samples.

Here, we construct a flexible ssDNA-SWNT electrochemical biosensor for high sensitivity and stability detection of cancer-relevant miRNA-21 in human urine samples to achieve bladder cancer (BCa) diagnosis and classification (Scheme 1). The 2D

Scheme 1. Schematic Illustration of ssDNA-SWNT Biosensors for the Detection of BCa-Relevant miRNA-21 in Human Urine to Achieve BCa Classification

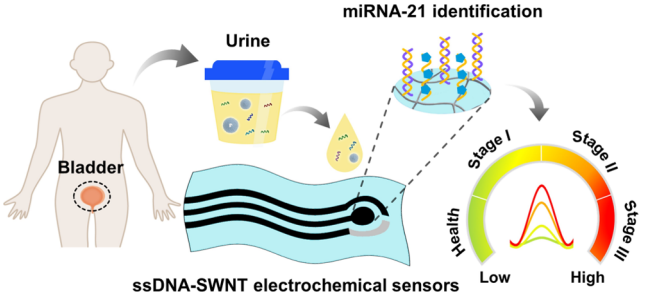

interconnected network structured ssDNA-SWNT electrodes with excellent conductivity enable the ultra-sensitive detection of miRNA-21 with a detection limit of 3.0 fM. Additionally, the intrinsic flexibility of ssDNA-SWNT electrodes can help maintain the electrical conductivity of the 2D interconnected network structure, ensuring the high stability detection of miRNA-21 even when the electrode was exposed to large bending deformations. The excellent detection reproducibility promises the potential of flexible electrochemical electrodes in POCT applications. Because urinary miRNA-21 is closely related to the progression and metastasis of BCa,[33] the relationship between urinary miRNA-21 levels and the status of BCa was investigated with the ssDNA-SWNT electrodes. In a cohort of 40 BCa patients at stages I–III and 44 negative control samples, the constructed ssDNA-SWNT biosensors could detect BCa with a 92.5% sensitivity, an 88.6% specificity, and classify the cancer stages with an overall accuracy (ACC) of 81.0%. With excellent detection sensitivity and stability, the ssDNA-SWNT biosensors can be adopted for treatment efficiency assessment. Overall, the design of flexible network structured ssDNA-SWNT electrochemical biosensors offers efficient strategies for point-of-care detection of complex clinical biological samples to achieve personalized diagnosis and surgical management.

EXPERIMENTAL SECTION

Chemicals and Reagents. Ethanol, acetone, hydrogen peroxide (H_2O_2, 30%), concentrated nitric acid (HNO_3, 65–68%), *N*-hydroxy succinimide (NHS, 98%), and 1-ethyl-(3-dimethylamino-propyl) carbodiimide hydrochloride (EDC, 98%) were purchased from Sinopharm Chemical Reagent Co. Ltd. Dimethylbenzene (C_8H_{10}), ferrocene ($C_{10}H_{10}Fe$), sublimated sulfur (S, 99.99%), methylene blue (MB), urea (CH_4N_2O), uric acid ($C_5H_4N_4O_3$), glucose ($C_6H_{12}O_6$), ascorbic acid ($C_6H_8O_6$), and 2-(*N*-morpholine) ethyl sulfonic acid buffer solution (MES, 500 mM, pH = 6.1) were obtained from Aladdin (Shanghai, China). Polyvinyl chloride (PVC) tapes (thickness, 0.15 mm) were purchased from Junye Adhesive Tape Technology Co., Ltd. (Shenzhen, China). The phosphate-buffered saline (PBS, 50 mM, pH = 7.4) was purchased from Shanghai Yuanye Bio-Technology Co., Ltd. All reagents were used without further purification. Deionized water (resistivity of 18.25 mΩ) was used throughout all the experiments. All the nucleotides were purchased from Sangon Biotechnology (Shanghai, China), and the corresponding sequences are listed in Table S1.

Apparatus and Characterizations. The morphology and microstructures of the SWNT electrodes were characterized by a high-resolution field emission scanning electron microscope (FEI Verios 460, America) and transmission electron microscopy (TEM) (JEOL, JEM-2100, Japan). Atomic force microscopy (AFM) (Park nx10, Korea) was used to characterize the surface and thickness of the ssDNA-SWNT electrodes. The attenuated total reflection Fourier transform infrared (ATR–FTIR) analysis was performed on a Bruker PMA 50 infrared spectrometer. The laser confocal Raman spectra of the SWNTs and ssDNA-SWNT electrodes were collected by a Renishaw inVia-Plus Raman microscope with excitation at 532 nm. The hydrophilic/hydrophobic of SWNT-based electrodes was measured using the contact angle OCA20 (Dataphysics, Germany). The pattern of electrode arrays was etched by a plasma cleaner (JSVAC-P200, China). A laser engraving machine (JL-K3020, China) equipped with a 50 W CO_2 laser was used for cutting user-designed PVC tape patterns. Cyclic voltammetry (CV), differential pulse voltammetry (DPV), and electrochemical impedance spectroscopic (EIS) measurements were performed by a CHI660E electrochemical workstation (Chenhua, Shanghai, China).

Synthesis of SWNT Membranes. SWNT membranes were synthesized by an atmospheric pressure chemical vapor deposition approach with the mixture solution of dimethylbenzene (1 mL) as precursor and ferrocene/sulfur (0.045/0.001 g) as catalysts according to previous reports.[34] H_2O_2 (30%) and concentrated HNO_3 were used to purify SWNT membranes to remove the impurities. In order to introduce carboxyl groups, SWNT membranes were immersed in concentrated HNO_3 and acidified for 72 h at 25 °C. The prepared SWNT membranes were cleaned with deionized water three times for subsequent use.

Preparation of Flexible SWNT Electrodes. The flexible SWNT electrode arrays were obtained by oxygen plasma etching of the SWNT membrane with the assistance of the PVC template. Specifically, a PVC template with electrode patterns was designed and fabricated by a laser-etching technique. The PVC template was then fixed on the surface of SWNT membranes. Subsequently, an O_2 plasma etching treatment (100 W, 40 Pa) was performed for 20 min to remove the exposed SWNTs to obtain SWNT electrodes arrays. Then, Ag/AgCl ink was applied to one of the SWNT electrodes to serve as the reference electrode. Consequently, the electrochemical electrodes with SWNTs as working and counter electrodes, and Ag/AgCl ink-coated SWNTs as reference electrodes were obtained.

Preparation of ssDNA-SWNT Electrodes. In order to obtain ssDNA-SWNT electrodes, ssDNA was introduced onto the SWNT electrodes. Briefly, the SWNT working electrode was exposed to a mixture solution including 5.0 mL of deionized water, 1.0 mL of 500 mM MES buffer solution, 2.0 mL of 50 mg/mL NHS aqueous solution, and 2.0 mL of 50 mg/mL EDC solution for 30 min at room temperature to activate carboxyl groups on the SWNT surface. Then, the SWNT electrodes were incubated with 1×10^{-5} M ssDNA in

https://doi.org/10.1021/acs.analchem.2c03156
Anal. Chem. 2023, 95, 1847–1855

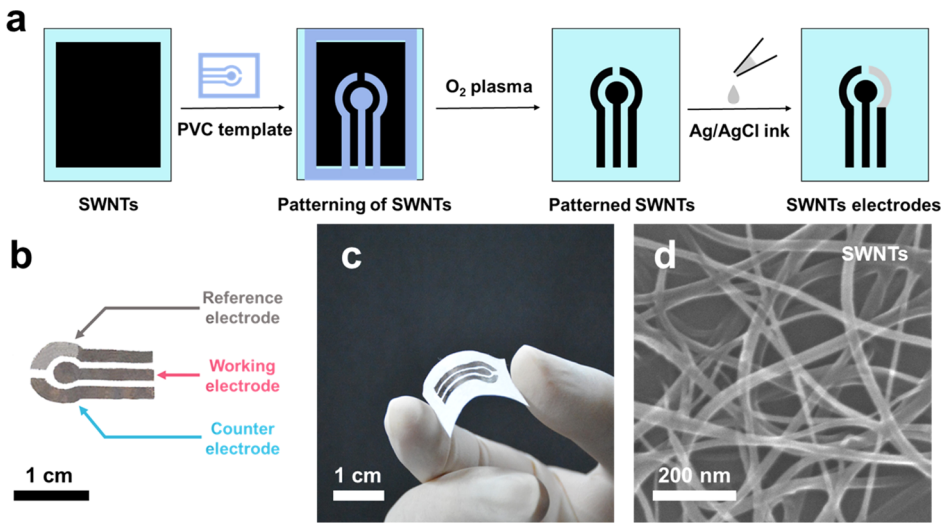

Figure 1. Fabrication and characterization of SWNT electrodes. (a) Schematic illustration of the fabrication process of flexible SWNT-based electrochemical electrodes. (b) Photograph of the SWNT-based electrochemical electrodes. (c) Optical image of the SWNT-based electrochemical electrodes under bending deformations. (d) SEM image of the SWNT electrodes.

1.0 mL of PBS buffer for 1 h at 35 °C. ssDNA-SWNT electrodes were finally obtained after being cleaned by PBS buffer three times.

miRNA-21 Measurements. To achieve the detection of miRNA-21 molecules, the ssDNA-SWNT electrodes were exposed to a series of miRNA-21 solutions with different concentrations and incubated at 35 °C for 30 min to fully hybridize miRNA-21 with ssDNA. MB, a typical hybridization indicator, was used as the signal label to examine the hybridization degree of nucleotides. Specifically, the electrodes were immersed into 2×10^{-5} mol/L MB solution and incubated for 5 min to load the redox tag MB. The electrochemical response of ssDNA-SWNT electrodes toward miRNA-21 was measured by DPV with a step increment of 5 mV, an amplitude of 50 mV, and a pulse period from −0.6 to 0 V (vs Ag/AgCl). The recovery of the electrodes was measured by adding different amounts of miRNA-21 into the human urine and recording the corresponding electrochemical response performance.

Clinical Samples Analysis. 50 human urine samples from BCa patients (40 for the identification of BCa stages, 10 for the monitoring of BCa status before and after surgical treatment), 14 from prostate cancer (PCa) patients and 6 from cystitis patients were provided by Union Hospital of Wuhan and Renmin Hospital of Wuhan University, and 30 human urine samples from healthy volunteers were collected from the College of Chemistry and Molecular Sciences of Wuhan University. All participants sign in the informed consent before being involved in this study. All procedures performed in this study involving human participants were in accordance with the ethical standards of the institutional and/or national research committee. For the analysis of clinical samples, miRNA-21 in human urine samples was extracted using a typical extraction kit for liquid samples (Genebetter R214-50, China). The extracted miRNA-21 was diluted 40 times in PBS for electrochemical measurements. Receiver operating characteristic (ROC) curves were constructed for miRNA-21. Sensitivity describes the probability of the positive test result when cancer was detected (true positive rate). Specificity describes the probability of the negative test result when cancer was not detected (true negative rate). ACC describes the overall probability that an individual was classified correctly. The 95% confidence intervals (CIs) were calculated with a binomial distribution.[35]

RESULTS AND DISCUSSION

Fabrication and Characterization of Flexible SWNT Electrodes. To achieve high sensitivity and stability detection of miRNA-21 in human urine samples, the flexible SWNT electrochemical electrodes were first fabricated as schematically illustrated in Figure 1a. Briefly, the CVD grown SWNT membrane was transferred onto a flexible substrate to serve as the starting material. A user-defined pattern, cut by the laser engraving technique on a PVC tape, was then attached to the surface of the SWNTs membrane. Subsequently, an O_2 plasma process was applied to remove the exposed SWNTs and patterned SWNT electrodes were obtained. The SWNT-based electrochemical electrodes were fabricated after coating Ag/AgCl ink onto one of the SWNT electrode surfaces to serve as the reference electrode. The flexible ssDNA-SWNT electrodes could be readily scaled up because there is no fundamental limitation in fabricating a large-area uniform SWNT membrane. As shown in Figure 1b, the SWNT-based electrochemical electrodes with three electrodes including a reference electrode, a working electrode, and a counter electrode were fabricated. The SWNT-based electrochemical electrodes could sustain large bending deformations without compromising the structural integrity, indicating that the SWNT electrodes exhibit excellent mechanical flexibility (Figure 1c). Scanning electron microscopy (SEM) and TEM characterizations were utilized to investigate the morphology and structure of the fabricated SWNT electrodes. As shown in Figures 1d and S1, the SEM and TEM images of the SWNT electrode clearly reveal the 2D porous interconnected network structure that is woven by 1D SWNTs. The above results demonstrate that flexible network structured SWNT electrodes cross-linked with conductive 1D SWNTs were successfully fabricated.

Fabrication and Characterization of ssDNA-SWNT Biosensors. To fabricate ssDNA-SWNT electrochemical biosensors, the recognition molecules ssDNA with the capability to identify target miRNA-21 in human urine samples

https://doi.org/10.1021/acs.analchem.2c03156
Anal. Chem. 2023, 95, 1847−1855

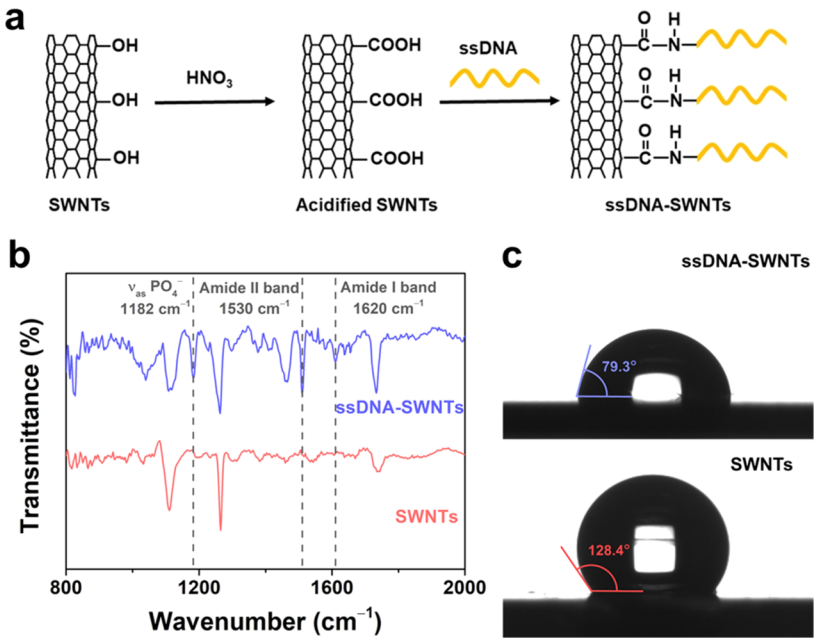

Figure 2. Fabrication and characterization of ssDNA-SWNT biosensors. (a) Schematic illustration of the fabrication process of ssDNA-SWNT working electrodes. (b) ATR−FTIR spectra of the flexible ssDNA-SWNTs (blue) and bare SWNTs (red) electrodes. (c) Contact angles of flexible ssDNA-SWNTs and SWNT electrodes.

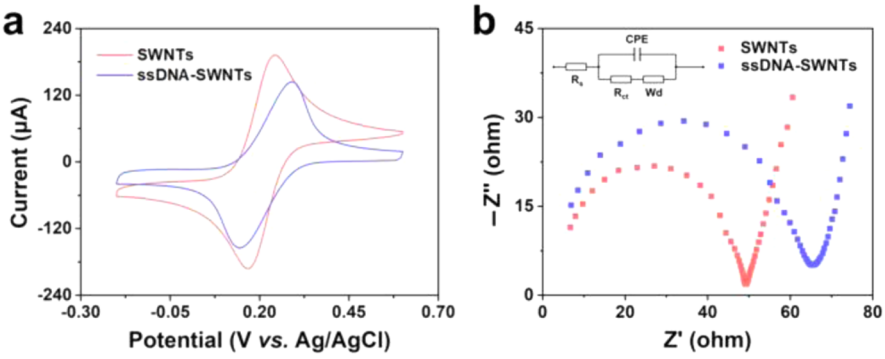

Figure 3. Electrochemical characterization of ssDNA-SWNT electrodes. (a) CV and (b) EIS curves of the ssDNA-SWNT (blue) and SWNT (red) electrodes.

were functionalized on the working electrode of flexible SWNT-based electrochemical electrodes. As schematically illustrated in Figure 2a, the SWNT working electrode was first treated with concentrated HNO_3 to introduce carboxyl groups on the SWNT surface. Then, amine-terminated ssDNA, to identify miRNA-21, was conjugated with carboxyl groups on the SWNT working electrodes through the formation of amide bonds. To investigate the conjugation efficiency of ssDNA on the SWNT working electrode, ATR−FTIR spectroscopy was performed. As shown in Figure 2b, the peak of the anti-symmetric phosphate backbone (ν_{as} PO^{4-}) ascribed to ssDNA appears at 1182 cm^{-1} in the spectra of ssDNA-SWNTs. In addition, the presence of peaks at 1530 and 1620 cm^{-1} assigned to amide II and amide I indicate the formation of amide bonds after ssDNA modification.[36,37] These results suggest that ssDNA probes were successfully functionalized on the SWNT working electrode. The hydrophobic/hydrophilic characters of the SWNT working electrode were evaluated with contact angle measurements. As shown in Figure 2c, the ssDNA-SWNT and SWNT electrodes exhibit average contact angles of 79.3 and 128.4°, respectively, suggesting that the attachment of ssDNA enables the SWNTs to be hydrophilic. The hydrophilic characters of the ssDNA-SWNT electrodes would facilitate the efficient detection of biomolecules in a liquid environment.[38] After the modification of ssDNA, the SWNT working electrodes exhibit an average thickness of 75 nm, as shown in the AFM height profile (Figure S2). Moreover, the SWNT working electrodes maintain the porous network structure well after conjugation with ssDNA (Figure S3). The Raman spectra of ssDNA-SWNT electrodes in Figure S4 shows negligible peak shifts compared with bare SWNT electrodes, indicating that the intrinsic structure of SWNTs retains after ssDNA modification.[39] The above structure characterizations of the ssDNA-SWNT working electrodes demonstrate that the network structure of SWNTs electrodes was well maintained after ssDNA immobilization.

Electrochemical Characterization of ssDNA-SWNT Electrodes. The electrochemical performance of ssDNA-SWNT electrodes was evaluated by CV in the presence of 5 mM ferrocyanide/ferricyanide ($[Fe(CN)_6]^{4-}/[Fe(CN)_6]^{3-}$). The scan rate was fixed at 50 mV/s. As shown in Figure 3a, compared to bare SWNT electrodes, the flexible ssDNA-

https://doi.org/10.1021/acs.analchem.2c03156
Anal. Chem. 2023, 95, 1847−1855

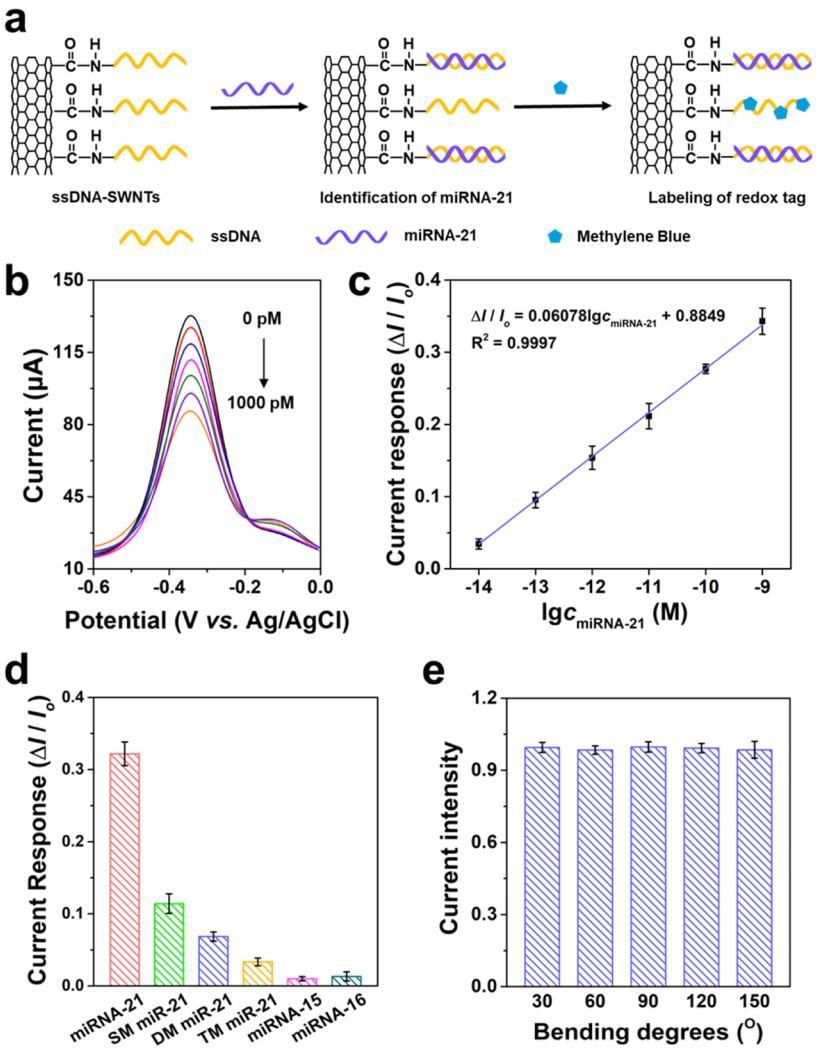

Figure 4. miRNA-21 detection performance evaluation. (a) Schematic illustration of the detection of miRNA-21 with flexible ssDNA-SWNT biosensors. (b) DPV curves of flexible ssDNA-SWNT biosensors toward different concentrations of miRNA-21. (c) Calibration curve of flexible ssDNA-SWNT biosensors for miRNA-21. (d) Current responses of flexible ssDNA-SWNT biosensors toward target miRNA-21 and interfering molecules including SM miR-21, DM miR-21, TM miR-21, miRNA-15, and miRNA-16. (e) Current intensity of flexible ssDNA-SWNT biosensors for miRNA-21 under different bending deformations.

SWNT electrodes exhibit a decreased peak current, which can be attributed to electrostatic repulsion between negatively charged ssDNA and $[Fe(CN)_6]^{3-}$.[40] In addition, EIS was performed to track the changes in the charge transfer resistance (R_{ct}) of the ssDNA-SWNT electrodes. As shown in Figure 3b, the flexible ssDNA-SWNT electrode exhibits an enlarged diameter compared with that of bare SWNT electrodes in the high-frequency region, indicating that the R_{ct} of SWNT electrodes was increased after the modification of ssDNA. The electrical conductivity of the flexible ssDNA-SWNT electrodes plays a critical role in the signal conduction of electrochemical biosensors.[41] As shown in Figure S5, it can be calculated that the absolute value of the slope of the current−voltage ($I-V$) curve is 25.4 mA/V. Accordingly, the conductivity of the flexible ssDNA-SWNT electrode was calculated to be 3.1×10^5 S/m, which is superior to previously reported electrodes such as indium tin oxide (1.9×10^4 S/m),[42] graphene (5.5×10^4 S/m),[43] and inorganic graphene analogues (5.0×10^2 S/m).[44] With excellent electrical conductivity, the fabricated ssDNA-SWNT electrodes are promising for the highly sensitive detection of miRNA-21.

Detection of miRNA-21. The occurrence and development of BCa are associated with miRNA-21 in human urine.[45−48] The capability of flexible ssDNA-SWNT biosensors for miRNA-21 identification was investigated as schematically illustrated in Figure 4a. To be specific, the miRNA-21 targets could be hybridized with the complementary ssDNA on the SWNTs via the formation of Hoogsteen base pairs. MB was adopted as redox tags to examine the hybridization degree of nucleotides. In the presence of miRNA-21 targets, the interaction between the redox tag MB and the flexible ssDNA-SWNT electrode weakened owing to the reduced exposed bases in ssDNA, resulting in a decrease in the response current of MB on the electrode, thus realizing the detection of miRNA-21 (Figure S6).[49] Before the miRNA-21 measurements, the measurement conditions including hybridization time, hybridization temperature and concentration of MB were optimized (Figure S7). Under the optimized conditions, DPV measurements were carried out with the constructed flexible ssDNA-SWNT electrochemical biosensors. As displayed in Figure 4b, the current signal intensity decreases with the increase of miRNA-21 concentration. Meanwhile, the

https://doi.org/10.1021/acs.analchem.2c03156
Anal. Chem. 2023, 95, 1847−1855

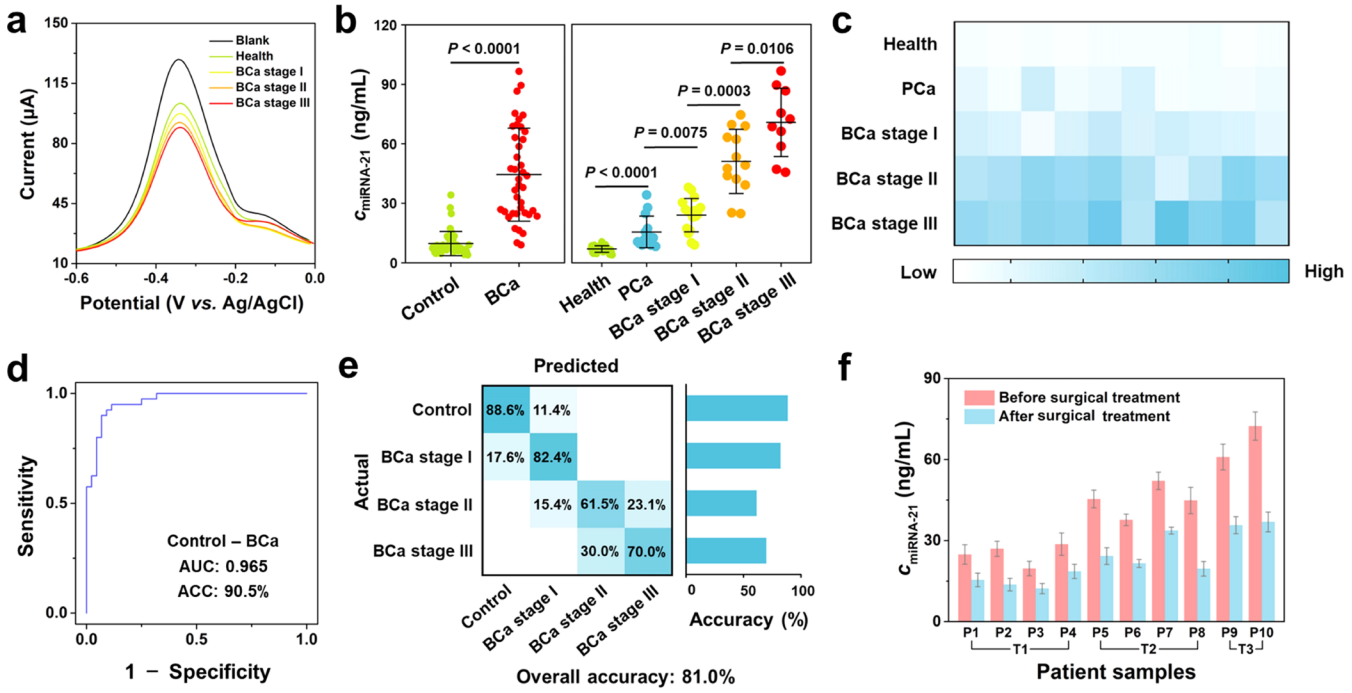

Figure 5. Analysis of urinary miRNA-21 levels in clinical samples. (a) DPV curves of flexible ssDNA-SWNT biosensors toward human urine samples from healthy individuals and BCa patients at stages I, II, and III. (b) Calculated miRNA-21 concentration of human urine samples from healthy individuals, PCa patients, and BCa patients at stages I, II, and III. (c) Heat map of miRNA-21 profiles in a cohort [n = 50; i.e., 30 for BCa patients at stages I, II, and III (10 per cancer stage), 10 for PCa patients, and 10 for healthy individuals]. (d) ROC curve of the flexible ssDNA-SWNT biosensors in differentiating negative control samples and BCa patients. (e) Confusion matrix summarizing the cancer classification results in a validation cohort. (f) Measured miRNA-21 concentration before and after surgical treatment with flexible ssDNA-SWNT biosensors.

linear relationship between the current signal intensity and the logarithmic of miRNA-21 concentration indicates that the dynamic range is 10^{-14} to 10^{-9} M (Figure 4c). Specifically, the linear regression equation could be expressed as follows: $\Delta I/I_0 = 0.0608 \log c + 0.8849$, with a correlation-coefficient value R^2 of 0.9997. The detection limit is calculated to be 3.0 fM (limit of detection (LOD) = 3 S_b/m, S_b represents the standard deviation of blank signals, m represents the slope of the fitted curve), and this value is particularly lower than the miRNA-21 level (~pM) in BCa patients. To evaluate the detection performance of flexible ssDNA-SWNT biosensors, the detection limit was compared with previously reported biosensors (Table S2). It can be seen that the flexible ssDNA-SWNT biosensors in our work show excellent sensitivity with an extremely low LOD of 3.0 fM compared with previously reported luminescence and electrochemical biosensors for miRNA-21 detection.

Considering the complexity of biological samples, the selectivity of ssDNA-SWNT biosensors was investigated. To be specific, SM miR-21, DM miR-21, TM miR-21, miRNA-15, and miRNA-16 were chosen as the interfering molecules. As shown in Figures 4d and S8, the interfering molecules with a concentration of 10^{-9} M all show considerable low electrochemical current responses compared with that of target miRNA-21, suggesting that the flexible ssDNA-SWNT biosensors exhibit high selectivity for target miRNA-21 over mismatched sequences. Besides, the electrochemical response of ssDNA-SWNT biosensors toward interfering molecules such as carbamide, uric acid, glucose, and ascorbic acid in complex urine environments is negligible, further demonstrating the excellent selectivity of flexible ssDNA-SWNT biosensors for miRNA-21 detection (Figure S9).

To assess the reliability of the ssDNA-SWNT biosensors for miRNA-21 identification, the detection stability, reproducibility, and recovery were investigated. As shown in Figure 4e, the electrochemical response of flexible ssDNA-SWNT biosensors toward miRNA-21 remains stable after bending at different angles, which can be ascribed to the porous networked structure of the flexible ssDNA-SWNT biosensors. Also, after storage for different time intervals, the ssDNA-SWNT biosensors maintain a relatively stable electrochemical response, further proving the excellent stability of the biosensors (Figure S10). These results validate that the constructed flexible ssDNA-SWNT biosensors exhibit excellent detection stability, and this feature could satisfy the requirements of portable, wearable, remote, and timely detection characteristics in practical POCT applications. The reproducibility was investigated by testing a same miRNA-21 sample with five ssDNA-SWNT biosensors. As shown in Figure S11, the standard deviation of five parallel tests is 4.63%, suggesting that the ssDNA-SWNT biosensors exhibit excellent detection reproducibility. The recovery investigations were performed by adding a series of miRNA-21 with concentrations of 0.1, 1, 10, 100, and 1000 pM into human urine samples to estimate the potential of flexible ssDNA-SWNT biosensors for miRNA-21 detection in real samples (Figure S12). The measured recovery rate varies between 95.6 and 107.0% (Table S3). The above investigations indicate that the flexible ssDNA-SWNT biosensors show great potential for miRNA-21 detection in practical biological samples.

Clinical Samples Measurements and Cancer Classifications. Urinary miRNA-21 plays a crucial role in the development, progression, and metastasis of BCa, and it shows an upregulated expression in the urine of BCa patients.[50,51]

https://doi.org/10.1021/acs.analchem.2c03156
Anal. Chem. 2023, 95, 1847−1855

Therefore, the detection of urinary miRNA-21 level is crucial for the pathological evaluation and prognosis monitoring of BCa. To investigate the clinical application potential of flexible ssDNA-SWNT biosensors, human urine samples from 40 BCa patients at stages I−III and 44 negative control samples (including 30 from healthy individuals and 14 from PCa patients) were collected and investigated (Tables S4−S7). As shown in Figure 5a, the electrochemical response of flexible ssDNA-SWNT biosensors differs among BCa patients and healthy individuals, demonstrating that the flexible ssDNA-SWNT biosensors could be utilized to identify miRNA-21 in human urine samples. The whole detection process for clinical urine samples just needs 20 min. Based on the electrochemical response and the calibrated response curves in Figure 4c, the concentration of miRNA-21 in human urine samples was calculated and summarized in Figure 5b and Table S8. As shown in Figure 5b, the average concentration of urinary miRNA-21 is higher in BCa patients than in negative control samples. Because the clinical symptoms of PCa and BCa are similar, the urinary miRNA-21 in the corresponding human urine samples measured by ssDNA-SWNT biosensors is also plotted in Figure 5b. It can be observed that the urine samples in BCa patients show an obviously increased miRNA-21 level compared with that of PCa, suggesting that ssDNA-SWNT biosensors could achieve preliminary differentiation between PCa and BCa. The reason lies in the fact that the bladder tumor cells were directly in contact with urine and the bladder tumor relevant biomarkers could be released into urine pathologically, while the prostate tumor cells were blocked by urethral mucosa and early PCa is generally difficult to break through the urethral mucosa to release biomarkers into urine. As PCa progresses, locally advanced PCa is aggressive and destructive to urethral mucosa, and PCa relevant biomarkers would be released into urine. The ssDNA-SWNT biosensors could not distinguish between cystitis patients and BCa patients well due to the difficulty in accurately identifying different diseases with a single biomarker (Figure S13).[50,52] From Figure 5c, it can be observed that the miRNA-21 concentration increases with the BCa stages, which is consistent with the upregulated expression theory of BCa.[45,50] This result suggests that the flexible ssDNA-SWNT biosensors might be utilized to give a discrimination. To clearly investigate the differentiation capability of the flexible ssDNA-SWNT biosensors, the ROC analysis was performed (Figure 5d). A cutoff value (15.00 ng/mL) that could maximize the detection sensitivity and specificity was exploited for the differentiation of BCa and negative controls. As indicated in Figure 5d, the flexible ssDNA-SWNT biosensors show a sensitivity of 92.5%, a specificity of 88.6%, an ACC of 90.5%, and an area under the curve of 0.965 for BCa versus control. The ACC of 90.5% is much higher than that of 62.5% measured with the clinical fluorescent in situ hybridization (FISH) technique (Table S9). Subsequently, the cancer stages classification results were summarized into a confusion matrix. As shown in Figure 5e, 82.4, 61.5, and 70.0% of stages I, II, and III BCa could be accurately identified and an overall ACC of 81.0% (95% CI: 76.7−85.3%) was obtained for cancer stages classification. It is worth mentioning that the higher identification ACC for stage I BCa compared to stage II and stage III BCa is due to the fact that the miRNA-21 expression level is significantly improved in BCa patients compared with that of negative controls, while the miRNA-21 levels between different cancer stages overlapped to some extent. The above results validate that the constructed flexible ssDNA-SWNT biosensors show the capability for cancer staging.

BCa is a type of cancer with a high recurrence rate after surgical treatment.[53−55] Hence, the monitoring of BCa patients is of vital importance to improve the survival rate.[56] The monitoring of BCa associated miRNA-21 in human urine samples might offer a pathway to achieve BCa prognosis. In this regard, the response performance of flexible ssDNA-SWNT biosensors toward urine samples from BCa patients before and after surgical treatment was investigated (Table S10). As shown in Figures 5f and S14, the concentration of miRNA-21 of all the investigated BCa patients obviously decreases after surgical treatment compared with that of before surgical treatment ($P < 0.05$, paired two-sided t-test). This result indicates that the flexible ssDNA-SWNT biosensors could provide an efficient strategy for treatment efficiency assessment and cancer recurrence monitoring. The flexible, portable, and highly sensitive ssDNA-SWNT biosensor design strategies in this work provide insights for practical POCT applications to achieve the prediction, diagnosis, monitoring, and staging of cancer.

CONCLUSIONS

In summary, a flexible ssDNA-SWNT electrochemical biosensor was established for high sensitivity and stability miRNA-21 detection in complex clinical urine samples to achieve BCa diagnosis and classifications. Owing to the 2D interconnected network structure with high electrical conductivity and flexibility, the ssDNA-SWNT biosensors enable the highly sensitive and stable detection of miRNA-21 even under large bending deformations. A detection limit of 3.0 fM and a wide linear range from 10^{-14} to 10^{-9} M were achieved with the flexible ssDNA-SWNT biosensors. Besides, the flexible ssDNA-SWNT biosensors exhibit excellent selectivity in the detection of miRNA-21. With excellent detection performance, the flexible ssDNA-SWNT biosensors could realize efficient miRNA-21 detection in complex clinical urine samples, showing a sensitivity of 92.5%, a specificity of 88.6%, and an ACC of 90.5% for BCa versus negative control. Additionally, the flexible ssDNA-SWNT biosensors could classify the cancer stages with an overall ACC of 81.0%. Moreover, our constructed flexible ssDNA-SWNT biosensors could also provide a way for treatment efficiency assessment and cancer recurrence monitoring. The flexible ssDNA-SWNT biosensors with high sensitivity offer an affordable, accessible solution for point-of-care detection and are promising in achieving the goal of health management and personalized medicine.

ASSOCIATED CONTENT

Supporting Information

The Supporting Information is available free of charge at https://pubs.acs.org/doi/10.1021/acs.analchem.2c03156.

TEM image of the SWNT electrode; AFM images and Raman spectra of ssDNA-SWNT electrodes; DPV curves of flexible ssDNA-SWNT biosensors toward MB molecules; optimization of experimental conditions for miRNA-21 detection; reproducibility, stability, anti-interference ability, and recovery measurements of flexible ssDNA-SWNT biosensors; expression level of miRNA-21 in BCa patients before and after surgical treatment; sequences of nucleic acids used in the

https://doi.org/10.1021/acs.analchem.2c03156
Anal. Chem. 2023, 95, 1847−1855

experiment; comparison of miRNA-21 detection performance; information statistics of negative controls and BCa patients; and information statistics of urine detection results obtained by the FISH technique (PDF)

AUTHOR INFORMATION

Corresponding Author

Yanbing Yang − *College of Chemistry and Molecular Sciences, School of Microelectronics, Wuhan University, Wuhan 430072, P. R. China*; Email: yangyanbing@whu.edu.cn

Authors

Duo Chen − *College of Chemistry and Molecular Sciences, School of Microelectronics, Wuhan University, Wuhan 430072, P. R. China*

Na Chen − *College of Chemistry and Molecular Sciences, School of Microelectronics, Wuhan University, Wuhan 430072, P. R. China*

Fangning Liu − *Urology Department, Union Hospital, Tongji Medical College of Huazhong Science and Technology University, Wuhan 430000, P. R. China*

Yiming Wang − *College of Chemistry and Molecular Sciences, School of Microelectronics, Wuhan University, Wuhan 430072, P. R. China*

Huageng Liang − *Urology Department, Union Hospital, Tongji Medical College of Huazhong Science and Technology University, Wuhan 430000, P. R. China*; orcid.org/0000-0001-7838-8701

Quan Yuan − *College of Chemistry and Molecular Sciences, School of Microelectronics, Wuhan University, Wuhan 430072, P. R. China; Molecular Science and Biomedicine Laboratory (MBL), State Key Laboratory of Chemo/Biosensing and Chemometrics, College of Chemistry and Chemical Engineering, Hunan University, Changsha 410082, P. R. China*; orcid.org/0000-0002-3085-431X

Complete contact information is available at: https://pubs.acs.org/10.1021/acs.analchem.2c03156

Author Contributions

‖D.C., N.C., and F.L. contributed equally to this work.

Notes

The authors declare no competing financial interest.

ACKNOWLEDGMENTS

The National Natural Science Foundation of China (21925401 and 21904033), the National Key R&D Program of China (2017YFA0208000 and 2021YFA1202400), the Fundamental Research Funds for the Central Universities (2042021kf0036 and 2042022kf0028), and the Tencent Foundation are acknowledged for research funding. We thank the Core Facility of Wuhan University for large-scale instrument and equipment sharing foundation.

REFERENCES

(1) Miller, A. M.; et al. *Nature* **2019**, *565*, 654−658.
(2) Shrivastava, S.; Trung, T. Q.; Lee, N. E. *Chem. Soc. Rev.* **2020**, *49*, 1812−1866.
(3) Tu, J.; Torrente-Rodríguez, R. M.; Wang, M.; Gao, W. *Adv. Funct. Mater.* **2019**, *30*, 1906713.
(4) Bury, D.; Martin-Hirsch, P. L.; Martin, F. L.; Dawson, T. P. *Lancet* **2017**, *390*, 2765−2766.
(5) Zong, C.; Xu, M.; Xu, L.-J.; Wei, T.; Ma, X.; Zheng, X.-S.; Hu, R.; Ren, B. *Chem. Rev.* **2018**, *118*, 4946−4980.
(6) Ji, C.; Tan, J.; Yuan, Q. *Chin. J. Chem.* **2021**, *39*, 3188−3198.
(7) Prattis, I.; Hui, E.; Gubeljak, P.; Kaminski Schierle, G. S.; Lombardo, A.; Occhipinti, L. G. *Trends Biotechnol.* **2021**, *39*, 1065−1077.
(8) Qi, L.; Yang, M.; Chang, D.; Zhao, W.; Zhang, S.; Du, Y.; Li, Y. *Angew. Chem., Int. Ed.* **2021**, *60*, 24823−24827.
(9) Pei, H.; Zuo, X.; Zhu, D.; Huang, Q.; Fan, C. *Acc. Chem. Res.* **2014**, *47*, 550−559.
(10) Liao, N.; Pan, M.-C.; Wang, L.; Yang, F.; Yuan, R.; Zhuo, Y. *Anal. Chem.* **2021**, *93*, 4051−4058.
(11) Liao, N.; Liu, J.-L.; Chai, Y.-Q.; Yuan, R.; Zhuo, Y. *Anal. Chem.* **2020**, *92*, 3940−3948.
(12) Liang, L.; Wang, M.; Lu, S.; Kong, M.; Lin, Y.; Cuzzucoli, F.; Wang, P.; Wang, S. *Anal. Chim. Acta* **2018**, *1044*, 93−101.
(13) Zhang, H.; Wang, Z.; Wang, F.; Zhang, Y.; Wang, H.; Liu, Y. *Anal. Chem.* **2020**, *92*, 5546−5553.
(14) Lin, M.; Yi, X.; Wan, H.; Zhang, J.; Huang, F.; Xia, F. *Anal. Chem.* **2020**, *92*, 9963−9970.
(15) Wester, N.; Mikladal, B. F.; Varjos, I.; Peltonen, A.; Kalso, E.; Lilius, T.; Laurila, T.; Koskinen, J. *Anal. Chem.* **2020**, *92*, 13017−13024.
(16) Wang, Y.; Li, Z.; Lin, Q.; Wei, Y.; Wang, J.; Li, Y.; Yang, R.; Yuan, Q. *ACS Sens.* **2019**, *4*, 2124−2130.
(17) Zhu, M.; Li, S.; Li, H.; Li, H.; Xia, F. *Anal. Chem.* **2020**, *92*, 12437−12441.
(18) Zhao, Z.; Huang, C.; Huang, Z.; Lin, F.; He, Q.; Tao, D.; Jaffrezic-Renault, N.; Guo, Z. *TrAC, Trends Anal. Chem.* **2021**, *139*, 116253.
(19) Wang, Y.; Zhou, J.; Li, J. *Small Methods* **2017**, *1*, 1700197.
(20) Zhao, M.-L.; Zeng, W.-J.; Chai, Y.-Q.; Yuan, R.; Zhuo, Y. *Anal. Chem.* **2020**, *92*, 11044−11052.
(21) Yu, H.; Chen, Z.; Liu, Y.; Alkhamis, O.; Song, Z.; Xiao, Y. *Angew. Chem., Int. Ed.* **2021**, *60*, 2993−3000.
(22) Dai, Y.; Liu, C. C. *Angew. Chem., Int. Ed.* **2019**, *58*, 12355−12368.
(23) Pei, H.; Lu, N.; Wen, Y.; Song, S.; Liu, Y.; Yan, H.; Fan, C. *Adv. Mater.* **2010**, *22*, 4754−4758.
(24) Cao, P.; Wang, N.; Dai, H.; Ma, H.; Lin, M. *Anal. Chim. Acta* **2021**, *1151*, 338251.
(25) Yang, Y.; Yang, X.; Yang, Y.; Yuan, Q. *Carbon* **2018**, *129*, 380−395.
(26) Yang, Y.; Yang, X.; Zou, X.; Wu, S.; Wan, D.; Cao, A.; Liao, L.; Yuan, Q.; Duan, X. *Adv. Funct. Mater.* **2017**, *27*, 1604096.
(27) Lee, J.; Llerena Zambrano, B.; Woo, J.; Yoon, K.; Lee, T. *Adv. Mater.* **2020**, *32*, No. e1902532.
(28) Ouyang, T.; Cheng, K.; Yang, F.; Zhou, L.; Zhu, K.; Ye, K.; Wang, G.; Cao, D. *J. Mater. Chem. A* **2017**, *5*, 14551−14561.
(29) Yang, T.; Deng, W.; Chu, X.; Wang, X.; Hu, Y.; Fan, X.; Song, J.; Gao, Y.; Zhang, B.; Tian, G.; Xiong, D.; Zhong, S.; Tang, L.; Hu, Y.; Yang, W. *ACS Nano* **2021**, *15*, 11555−11563.
(30) Zhang, S.; Liu, H.; Yu, J.; Li, B.; Ding, B. *Nat. Commun.* **2020**, *11*, 5134.
(31) Hu, A.; Pang, Q.; Tang, C.; Bao, J.; Liu, H.; Ba, K.; Xie, S.; Chen, J.; Chen, J.; Yue, Y.; Tang, Y.; Li, Q.; Sun, Z. *J. Am. Chem. Soc.* **2019**, *141*, 11322−11327.
(32) Li, G.-F.; Yang, D.; Abel Chuang, P.-Y. *ACS Catal.* **2018**, *8*, 11688−11698.
(33) Hirofumi, Y.; Naohiko, S.; Toshihiko, I.; Takeshi, C.; Masayuki, N.; Hideki, E. *Nat. Rev. Neurol.* **2013**, *10*, 396−404.
(34) Yang, Y.; Yang, X.; Liang, L.; Gao, Y.; Cheng, H.; Li, X.; Zou, M.; Ma, A.; Yuan, R.; Duan, Q.; Duan, X. *Science* **2019**, *364*, 1057−1062.
(35) Liu, C.; Zhao, J.; Tian, F.; Cai, L.; Zhang, W.; Feng, Q.; Chang, J.; Wan, F.; Yang, Y.; Dai, B.; Cong, Y.; Ding, B.; Sun, J.; Tan, W. *Nat. Biomed. Eng.* **2019**, *3*, 183−193.
(36) Krüger, A.; Bürkle, A.; Hauser, K.; Mangerich, A. *Nat. Commun.* **2020**, *11*, 2174.

(37) Schmidt, M. P.; Martínez, C. E. *Langmuir* **2017**, *33*, 8525−8532.
(38) Yang, M. Q.; Tan, C. F.; Lu, W.; Zeng, K.; Ho, G. W. *Adv. Funct. Mater.* **2020**, *30*, 2004460.
(39) Yang, X.; Yang, Y.; Fu, L.; Zou, M.; Li, Z.; Cao, A.; Yuan, Q. *Adv. Funct. Mater.* **2018**, *28*, 1704505.
(40) Dong, S.; Zhao, R.; Zhu, J.; Lu, X.; Li, Y.; Qiu, S.; Jia, L.; Jiao, X.; Song, S.; Fan, C.; Hao, R.; Song, H. *ACS Appl. Mater. Interfaces* **2015**, *7*, 8834−8842.
(41) Low, S. S.; Loh, H. S.; Boey, J. S.; Khiew, P. S.; Chiu, W. S.; Tan, M. T. T. *Biosens. Bioelectron.* **2017**, *94*, 365−373.
(42) Lee, J.; Lee, S.; Li, G.; Petruska, M. A.; Paine, D. C.; Sun, S. *J. Am. Chem. Soc.* **2012**, *134*, 13410−13414.
(43) Wang, X.; Zhi, L.; Müllen, K. *Nano Lett.* **2008**, *8*, 323−327.
(44) Lin, C.; Zhu, X.; Feng, J.; Wu, C.; Hu, S.; Peng, J.; Guo, Y.; Peng, L.; Zhao, J.; Huang, J.; Yang, J.; Xie, Y. *J. Am. Chem. Soc.* **2013**, *135*, 5144−5151.
(45) Guo, J.; Shen, R.; Shen, X.; Zeng, B.; Yang, N.; Liang, H.; Yang, Y.; Yuan, Q. *Chin. Chem. Lett.* **2022**, *33*, 979−982.
(46) Ordonez, J. M.; Serrano, M. J.; García-Puche, J. L.; Ortega, F. G.; Diaz-Monchon, J. J. Â.; Lorente, j. A.; Perez, D. d. M. *J. Clin. Oncol.* **2015**, *33*, No. e22025.
(47) Wu, J.; Zhou, X.; Li, P.; Lin, X.; Wang, J.; Hu, Z.; Zhang, P.; Chen, D.; Cai, H.; Niessner, R.; Haisch, C.; Sun, P.; Zheng, Y.; Jiang, Z.; Zhou, H. *Anal. Chem.* **2021**, *93*, 8799−8809.
(48) Smith, D. A.; Newbury, L. J.; Drago, G.; Bowen, T.; Redman, J. E. *Sens. Actuators, B* **2017**, *253*, 335−341.
(49) Lu, Q.; Su, T.; Shang, Z.; Jin, D.; Shu, Y.; Xu, Q.; Hu, X. *Biosens. Bioelectron.* **2021**, *184*, 113229.
(50) Duan, R.; Zhang, Z.; Zheng, F.; Wang, L.; Guo, J.; Zhang, T.; Dai, X.; Zhang, S.; Yang, D.; Kuang, R.; Wang, G.; He, C.; Hakeem, A.; Shu, C.; Yin, P.; Lou, X.; Zeng, F.; Liang, H.; Xia, F. *ACS Appl. Mater. Interfaces* **2017**, *9*, 23420−23427.
(51) Catto, J. W. F.; Alcaraz, A.; Bjartell, A. S.; De Vere White, R. D. V.; Evans, C. P.; Fussel, S.; Hamdy, F. C.; Kallioniemi, O.; Mengual, L.; Schlomm, T.; Visakorpi, T. *Eur. Urol.* **2011**, *59*, 671−681.
(52) Yang, Y.; Wang, J.; Huang, W.; Wan, G.; Xia, M.; Chen, D.; Zhang, Y.; Wang, Y.; Guo, F.; Tan, J.; Liang, H.; Du, B.; Yu, L.; Tan, W.; Duan, X.; Yuan, Q. *Adv. Mater.* **2022**, *34*, 2203224.
(53) Yang, Y.; Zeng, B.; Li, Y.; Liang, H.; Yang, Y.; Yuan, Q. *Sci. China: Chem.* **2020**, *63*, 997−1003.
(54) Lee, E.; Reed, G.; Dandawate, P.; Kaushik, G.; Subramaniam, D.; Holzbeierlein, J. M.; Anant, S.; Weir, S. J. *J. Clin. Oncol.* **2018**, *36*, 521.
(55) Li, Y.; Zeng, B.; Yang, Y.; Liang, H.; Yang, Y.; Yuan, Q. *Chin. Chem. Lett.* **2020**, *31*, 1387−1391.
(56) Ploussard, G.; Daneshmand, S.; Efstathiou, J. A.; Herr, H. W.; James, N. D.; Rödel, C. M.; Shariat, S. F.; Shipley, W. U.; Sternberg, C. N.; Thalmann, G. N.; Kassouf, W. *Eur. Urol.* **2014**, *66*, 120−137.

https://doi.org/10.1021/acs.analchem.2c03156
Anal. Chem. 2023, 95, 1847−1855